Climate Dynamics
https://doi.org/10.1007/s00382-023-06807-6

The synergistic effect of the summer NAO and northwest pacific SST on extreme heat events in the central–eastern China

Hao Wang[1] · Jianping Li[1,2] · Fei Zheng[3,4] · Fei Li[1]

Received: 4 December 2022 / Accepted: 24 April 2023

Abstract
Extreme heat events happen frequently in East Asia, and may cause great damage to the ecosystem and society. The synergistic effect of the summer positive North Atlantic Oscillation (pNAO) and positive northwest Pacific (pNWP) sea surface temperature anomaly (SSTA) on the interannual variability of the extreme heat events in the central–eastern China (CEC) is investigated in this study. The two factors act synergistically in strengthening the extreme heat events in the CEC via a series of atmospheric bridges, and the CEC is likely to experience a hotter summer when both the summer pNAO and pNWP SSTA occur. The pNWP SSTA increases the strength of pNAO via the eastward propagating Rossby wave from the western Pacific. The enhanced pNAO induces a stronger eastward Rossby wave propagation across the Eurasian continent, and leads to a strong anomalous anticyclone over the CEC. The significantly increased atmosphere thickness increases the air temperature of the layer, and favors the extreme heat events in the CEC. Besides, the pNWP SSTA also has adjacent effect on the atmospheric circulation over the CEC, which could lead to a positive geopotential height anomaly. Therefore, the summer pNAO and pNWP SSTA act synergistically in influencing the atmospheric circulation over the CEC, and thereby significantly increase the extreme heat events in the CEC.

Keywords Extreme heat events · East Asia · China · North Atlantic Oscillation · Northwest pacific · Synergistic effect

1 Introduction

Under the background of global warming, extreme heat events happen more frequently than before, and the intensity of extreme heat events sees an increase in recent decades (Meehl and Tebaldi 2004; Perkins 2015; Fragkoulidis et al. 2018; Kornhuber et al. 2019). In the summer of 2022, China experienced record-breaking extreme heat events, and many stations in the Eastern and central-western China recorded the highest daily temperature in the history of the record. The frequent occurrence of extreme heat events which are often accompanied by drought and desertification has great impacts on the ecosystems, crop production and even humankind health (Alessandro and de Garín 2003; Bastos et al. 2014; Russo et al. 2015; Horton et al. 2016; Deng et al. 2018). The central–eastern China (CEC) is among the most heavily populated area, which is also the economic center in China, and the increase of extreme heat events may lead to huge negative impacts on the economy and society in this region (Sun et al. 2014; You et al. 2017).

The extreme heat events in the CEC have received a lot of attentions across many research fields in recent years, and it is of great importance to investigate the climatic mechanisms behind the extreme heat events in the CEC (e.g. Tan et al. 2007; Wu et al. 2012; Peng 2014). The extreme heat events can be caused by various factors, and the most common large-scale atmospheric circulation responsible for the extreme heat events is the anomalous anticyclone, which

✉ Jianping Li
ljp@ouc.edu.cn

✉ Fei Zheng
zhengf35@mail.sysu.edu.cn

1 Frontiers Science Center for Deep Ocean Multispheres and Earth System-Key Laboratory of Physical Oceanography-Institute for Advanced Ocean Studies-Academy of the Future Ocean, Ocean University of China, Qingdao 266100, China

2 Laoshan Laboratory, Qingdao 266237, China

3 School of Atmospheric Sciences, Ministry of Education, Key Laboratory of Tropical Atmosphere-Ocean System, Sun Yat-sen University, Zhuhai 519082, China

4 Southern Marine Science and Engineering Guangdong Laboratory, Zhuhai 519082, China

Published online: 03 May 2023

could reduce the cloud cover and increase the solar radiation (Black et al. 2004; Gershunov et al. 2009; Chen and Lu 2015; Lu and Chen 2016), and the atmosphere thickness change related to the anomalous atmospheric circulation can significantly influence the intensity and frequency of the extreme temperature events (Li et al. 2021). Gong et al. (2004) found that the anomalous high in the 500-hPa level is able to cause high temperature events in the CEC. Ding and Ke (2015) examined the extreme heat events in 2003 and 2013, and discovered that the extreme heat events in the eastern China could be related with the westward extended subtropical high with stronger intensity. Chen and Lu (2015) categorized the synoptic circulation related to the extreme heat events in the CEC into three patterns, and the most typical pattern is characterized by an anomalous anticyclone over the CEC.

The North Atlantic oscillation (NAO) is one of the most important atmospheric patterns, and it is the dominant mode of atmospheric circulation variability over the North Atlantic (Wallace and Gutzler 1981; Hurrell 1995; Li and Wang 2003). Previous studies found that the summer NAO is able to have impacts on the atmospheric circulation over East Asia via Rossby wave (Watanabe 2004; Chen et al. 2005; Zuo et al. 2015; Li and Ruan 2018). Xie et al. (2019) suggested that the NAO is able to modulate the surface air temperature over the East Asia on the decadal time scale via teleconnection, and the CEC is the most influenced region. The NAO is also found to influence air temperature and the resultant crop production in China through the upper-level Rossby wave (Sun et al. 2008; Zhou et al. 2013). Sun (2012) highlighted the effect of the summer NAO on the extreme heat events in the CEC, and the eastward propagated Rossby wave acts as the bridge between them.

The regional anomalous atmospheric circulation associated with the extreme heat events can also be modulated by many factors from the relatively adjacent regions. Many studies found that the decreased snow cover in the Tibetan Plateau could cause anomalous high pressure over the CEC, thus favors the extreme heat events (Sun et al. 2014; Wu et al. 2012). Deng et al. (2018) investigated the cause of the strong extreme heat event in southern China in 2018, and they discovered that the delayed South China Sea summer monsoon is the reason for it. Chen et al. (2016) found that the anomalous anticyclone caused by the boreal summer intraseasonal oscillation over the western Pacific can lead to heat waves in China. Zhu et al. (2012) highlighted the influence of the weakened East Asian summer monsoon on the extreme heat events. Hu et al. (2012) found that the late summer extreme heat events in the southern China can be affected by the Indian Ocean SST.

The northwestern Pacific (NWP) sea surface temperature (SST) is also an important adjacent factor influencing the climate in China. The NWP SST anomaly (SSTA) has important influence on the atmospheric circulation around China (e.g. Liu et al. 2006; Frankignoul et al. 2011; Matsumura et al. 2016). The NWP SST variability may influence the precipitation in the CEC by modulating the vapor transport (Li 2008; Li and Luo 2014). Previous studies suggested that the summer heat waves in the CEC could be caused by the NWP SSTA, since the NWP SST may force the anomalous atmospheric circulation over China (Chen and Zhou 2018; Sparrow et al. 2018). Huang et al. (2010) found that the NWP SST, which is near the eastern China, is able to modulate the summer extreme heat events in the CEC, and the positive NWP SSTA favors the increase of extreme heat events.

Since both the summer NAO and NWP SST may affect the variability of air temperature in the CEC respectively, we want to know that whether they have a combined effect on the interannual variability of the summer extreme heat events in the CEC. A new method was put forward by Li et al. (2019a) to determine the climatic synergistic effect of multiple factors, and this method was extensively used in previous studies. An et al. (2021) found that the Pacific and Atlantic SST could modulate the strength of circumglobal teleconnection and further influence the air temperature over the Mongolian Plateau. Sun and Li (2022) revealed that the wintertime precipitation over southeastern China and the Kuroshio Current in the East China Sea will be greatly enhanced if the El Niño and the positive phase of the North Pacific Oscillation both occur. Wang et al. (2022) explored the synergistic effect of the preceding winter positive phase of Northern Hemisphere Annular Mode and the spring negative phase of the tropical North Atlantic SST on weakening the spring extreme cold events in the mid-high latitudes of East Asia. Tang et al. (2022) revealed that the El Niño and negative phase of the NAO may lead to the significantly increased precipitation over the southeastern United States. Investigating of synergistic effect of the two factors may have great importance, since compared with single factor happening, the synergistic effect results in much greater amplitudes of the extreme events when two factors cooccur, which may cause more damage to the society and ecosystem. Thus, in this paper, we will focus on the synergistic effect of the summer NAO and NWP SST.

The remainder of this paper is organized as follows. The datasets and methodology are introduced in Sect. 2. Section 3 describes the characters of the synergistic effect of the summer positive NAO (pNAO) and positive NWP (pNWP) SSTA on the extreme heat events in the CEC. Section 4 presents the regional atmospheric circulation which is responsible for the extreme heat events in the CEC. Section 5 further explores the mechanisms of the synergistic effect. Finally, the summary and discussion are presented in Sect. 6.

2 Data and methods

2.1 Data

Table 1 lists all the datasets which are used in the study. The observational SST dataset is the HadISST1 (version 1.1) which is provided by the Met Office Hadley Center, and it has a horizontal resolution of a 1° latitude × 1° longitude and covers the period between January 1870 and July 2022 (Rayner et al. 2003). The HadEX3 dataset is employed to provide the gridded extreme temperature indices, and the dataset is provided by the Met Office Hadley Center covers the period 1901–2018 with a 1.25° latitude × 1.875° longitude grid (Dunn et al. 2020). The TXx, TNx, TX90p and TN90p indices are used in the dataset, and they represent the monthly highest value of the daily maximum temperature, monthly highest value of the daily minimum temperature, percentage of time when the daily maximum temperature is higher than the 90th percentile, and percentage of time when the daily minimum temperature is higher than the 90th percentile, respectively. The intensity and frequency of extreme heat events can be accurately represented by these indices (Dunn et al. 2020). The global surface air temperature time series of the HadCRUT4 dataset by the Met Office Hadley Center, which covers the period between January 1850 to January 2021 (Morice et al. 2012), is used to remove the global warming signal from all variables. The geopotential height, winds and sea level pressure (SLP) data are obtained from the National Centers for Environmental Prediction–National Center for Atmospheric Research (NCEP–NCAR) reanalysis dataset, which covers the period from 1948 to August 2022 on a 2.5° latitude × 2.5° longitude mesh (Kalnay et al. 1996).

The HadEX3 dataset ends in 2018, and has some missing data over East Asia before 1960. Therefore, the period 1961 – 2018 is used in this study.

2.2 Statistical methods

In this paper, summer is defined as June – July – August, and the two-tailed Student's *t* test is employed to determine statistical significance.

The synergistic effect diagnostic method used in this study is put forward by Li et al. (2019a). This method is able to determine the existence of synergistic effect statistically. Assuming there are two forcing factors F_1 and F_2, and each of the factors can be divided into positive, negative, and neutral phases. If we choose the positive phase of each factor, the conditions of the two factors will be represented as F_1^+ and F_2^+, representatively. $F_1^+ \oplus F_2^+$ denotes the cases with the cooccurrence of F_1^+ and F_2^+, and the cases are termed as joint events $F_1^+ \oplus F_2^+$. $F_1^+ \backslash F_2^+$ indicates the cases when F_1^+ occurs without F_2^+, and the cases are termed as single F_1^+ events. $F_2^+ \backslash F_1^+$ represents the cases when F_2^+ occurs without F_1^+, and the cases are termed as single F_2^+ events. Assuming the response T is investigated in the study, we can compare the difference between different events to determine whether there is a synergistic effect. If the $|T|$ of $F_1^+ \oplus F_2^+$ is greater than the maximum of the $|T|$ of $F_1^+ \backslash F_2^+$ and $F_2^+ \backslash F_1^+$, it denotes that there is a synergistic effect of F_1^+ and F_2^+ on T. However, if the $|T|$ of $F_1^+ \oplus F_2^+$ is smaller than the minimum of the $|T|$ of $F_1^+ \backslash F_2^+$ and $F_2^+ \backslash F_1^+$, it indicates that there is an antagonistic effect of F_1^+ and F_2^+. Finally, if the $|T|$ of $F_1^+ \oplus F_2^+$ is between the $|T|$ of $F_1^+ \backslash F_2^+$ and $F_2^+ \backslash F_1^+$, it indicates that there is no combined effect of F_1^+ and F_2^+. By using this synergistic diagnostic method, the existence of the synergistic effect of two factors can be determined.

The statistical significance of the synergistic effect is assessed by using the bootstrapping method (Deser et al. 2017, 2018). 1000 bootstrapped composites are formed based on joint events summer pNAO ⊕ pNWP, single summer pNAO events and single summer pNWP SSTA events. The bootstrapping method is used to test the difference between the joint events and single events by examining the distribution of 0 between the 10th and 95th percentiles. When 0 lies outside this area, the synergistic effect is

Table 1 Datasets employed in this study

Variable	Period of record	Spatial resolution	Source
SST	1870 – 3/2021	1° × 1°	HadISST1 (version 1.1) from the Met Office Hadley Center (Rayner et al. 2003)
Extreme temperature indices	1901 – 2018	1.25° × 1.875°	HadEX3 from the Met Office Hadley Center (Dunn et al. 2020)
Geopotential height, winds and sea level pressure	1949 – 5/2021	2.5° × 2.5°	National Centers for Environmental Prediction–National Center for Atmospheric Research (NCEP–NCAR) reanalysis version 1 (Kalnay et al. 1996)
The Global surface air temperature (SAT) time series	1850 – 1/2021	/	HadCRUT4 from Met Office Hadley Center (Morice et al. 2012)

significant. However, when 0 lies inside this area, the synergistic effect is insignificant.

The NAO index is calculated by the difference in the normalized regionally zonal-averaged SLP over the North Atlantic (80°W–30°E) between 35°N and 65°N according to Li and Wang (2003). All variables in the study are linearly detrended by removing the trends related to global warming in the global SAT time series of the HadCRUT4.

2.3 Dynamic analysis methods

The Rossby wave ray tracing theory in a horizontally non-uniform basic flow is performed to trace the trajectory of the stationary Rossby wave train and characterize the pathway of the impact of the NAO and NWP (Li and Li 2012; Li et al. 2015, 2019b, 2021; Zhao et al. 2015, 2019). The previous studies showed that the dispersion relationship of the Rossby wave frequency and wavenumber in a horizontally non-uniform flow can be written as (Karoly 1983; Li and Nathan 1997; Li and Li 2012; Li et al. 2015; Zhao et al. 2015, 2019):

$$\omega = \overline{u}_M k + \overline{v}_M l + \frac{\overline{q}_x l - \overline{q}_y k}{k^2 + l^2}, \tag{1}$$

where ω is the wave frequency; k and l are the zonal and meridional wavenumbers, respectively; $(\overline{u}_M, \overline{v}_M) = (\overline{u}, \overline{v})/\cos\varphi$ is the Mercator projection of zonal and meridional winds; φ is the latitude; $\overline{q} = \nabla_M^2 \overline{\psi}/\cos^2\varphi + f$ represents the absolute vorticity of the background; and $\overline{q}_x$ and $\overline{q}_y$ are the zonal and meridional gradients of $\overline{q}$. Let $K = \sqrt{k^2 + l^2}$ represent the total wavenumber, and the zonal and meridional components of the group velocity take the form:

$$u_g = \frac{\partial \omega}{\partial k} = \overline{u}_M + \frac{(k^2 - l^2)\overline{q}_y - 2kl\overline{q}_x}{K^4}, \tag{2}$$

$$v_g = \frac{\partial \omega}{\partial l} = \overline{v}_M + \frac{(k^2 - l^2)\overline{q}_x + 2kl\overline{q}_y}{K^4}. \tag{3}$$

The background flow changes along the ray, thus the wavenumbers determined by the kinematic wave theory can be written as (Whitham 1960):

$$\frac{d_g k}{dt} = -\frac{\partial \omega}{\partial x} = -k\frac{\partial \overline{u}_M}{\partial x} - l\frac{\partial \overline{v}_M}{\partial x} - \frac{1}{K^2}\left(l\frac{\partial \overline{q}_x}{\partial x} - k\frac{\partial \overline{q}_y}{\partial x}\right), \tag{4}$$

$$\frac{d_g l}{dt} = -\frac{\partial \omega}{\partial y} = -k\frac{\partial \overline{u}_M}{\partial y} - l\frac{\partial \overline{v}_M}{\partial y} - \frac{1}{K^2}\left(l\frac{\partial \overline{q}_x}{\partial y} - k\frac{\partial \overline{q}_y}{\partial y}\right), \tag{5}$$

where $\frac{d_g}{dt} = \frac{\partial}{\partial t} + \overline{u}_g\frac{\partial}{\partial x} + \overline{v}_g\frac{\partial}{\partial y}$ is the material derivative moving with the group velocity. According to Eqs. 4 and 5, the zonal and meridional wavenumbers change along the wave ray, which differs from the theory by Hoskins and Karoly (1981). Equations 2–5 are the wave ray tracing equation set. Therefore, the initial local meridional wave number l is determined by using Eq. (1) once the initial position and zonal wavenumber k are given. Then, the wave ray tracing equation set is able to obtain the corresponding wave ray trajectory. The integration is terminated when the local meridional wavelength is less than 1000 km in the large-scale Rossby wave.

The wave activity flux proposed by Takaya and Nakamura (2001) is also used in this study to identify the Rossby wave propagation, and the horizontal wave activity flux is calculated as the formula below:

$$\mathbf{W} = \frac{p\cos\varphi}{2|\overline{U}|}\begin{pmatrix} \frac{\overline{u}}{a^2\cos^2\varphi}\left[\left(\frac{\partial\psi'}{\partial\lambda}\right)^2 - \psi'\frac{\partial^2\psi'}{\partial\lambda^2}\right] + \frac{\overline{v}}{a^2\cos\varphi}\left[\frac{\partial\psi'}{\partial\lambda}\frac{\partial\psi'}{\partial\varphi} - \psi'\frac{\partial^2\psi'}{\partial\lambda\partial\varphi}\right] \\ \frac{\overline{u}}{a^2\cos\varphi}\left[\frac{\partial\psi'}{\partial\lambda}\frac{\partial\psi'}{\partial\varphi} - \psi'\frac{\partial^2\psi'}{\partial\lambda\partial\varphi}\right] + \frac{\overline{v}}{a^2}\left[\left(\frac{\partial\psi'}{\partial\varphi}\right)^2 - \psi'\frac{\partial^2\psi'}{\partial\varphi^2}\right] \end{pmatrix} \tag{6}$$

in this equation, ψ' indicates the perturbation stream function; $\overline{\mathrm{U}} = (\overline{u}, \overline{v})$ denotes the climatological mean wind velocity horizontal flow; p represents the pressure that is normalized by 1000 hPa; and a is the Earth's radium.

In order to study the effect of the anomalous atmospheric circulation on the air temperature anomaly, the perturbation hypsometric equation proposed by Li et al. (2021) is used:

$$\langle T\rangle' = \frac{g_0}{R}\left(\ln\frac{p_1}{p_2}\right)^{-1}\Delta Z'. \tag{7}$$

in this equation, $\langle T\rangle'$ is the anomaly of the mean temperature of the layer, $\Delta Z'$ is the atmospheric thickness anomaly between two pressure surfaces p_1 and p_2, g_0 is the gravitational acceleration, and R is the gas constant of dry air. It can be seen from the Eq. (7) that the perturbation mean air temperature of the atmospheric layer is proportional to the perturbation atmospheric thickness bounded by isobaric surfaces. Thus the atmospheric thickness anomaly can represent the perturbation mean air temperature of the atmospheric layer. The perturbation hypsometric equation is used to identify the effect of the upper-level atmospheric circulation anomaly on the air temperature variation.

We use a dry version of the linear baroclinic model (LBM) to investigate the influence of NAO and NWP SSTA on the atmospheric circulation. The LBM consists of primitive equations linearized of a summer climatology obtained from the NCEP–NCAR reanalysis dataset, and adopts a T21 horizontal resolution and 20 vertical levels using the sigma coordinate system. A further detailed description of the LBM can be found in Watanabe and Kimoto (2000). The

model is integrated for 35 days, and it takes about 20 days for the model to achieve a steady atmospheric circulation. The averaged result of days 26–35 is used in this study.

3 The synergistic effect of the summer NAO and NWP SST

Figure 1 shows the correlation maps between the summer NAO and extreme temperature indices in East Asia. Even though there are different extreme temperature indices, the significantly correlated area in China is always found in the CEC. The NAO shows a significantly positive correlation with the extreme heat events in the CEC, and it implies that the summer maximum daily temperature is higher than the climatology (Fig. 1c and d) and occurrence of hot days is more frequent when the summer pNAO happens (Fig. 1a and b). In other words, the occurrence of the summer pNAO is likely to be accompanied by the strengthened extreme heat events in the CEC (Sun 2012; Xie et al. 2019). Based on the results in Fig. 1, the region (25°–40°N, 110°–125°E) in the CEC is selected as the research area in this study.

Figure 2 further shows the time series of the summer area-averaged extreme heat indices in the CEC, and the pNAO years are marked on them. To include more cases, we use 0.6 standard deviations for the NAO index to select pNAO years (years with black dots in Fig. 2). It is clear that not every pNAO year exhibits strengthened extreme heat events in the CEC. Some pNAO years correspond to the significantly strengthened extreme heat events in the CEC (e.g. 1961, 1967 and 2013), while the slightly increased or even weakened extreme heat events occur in some pNAO years. This result could imply that there may be some factors

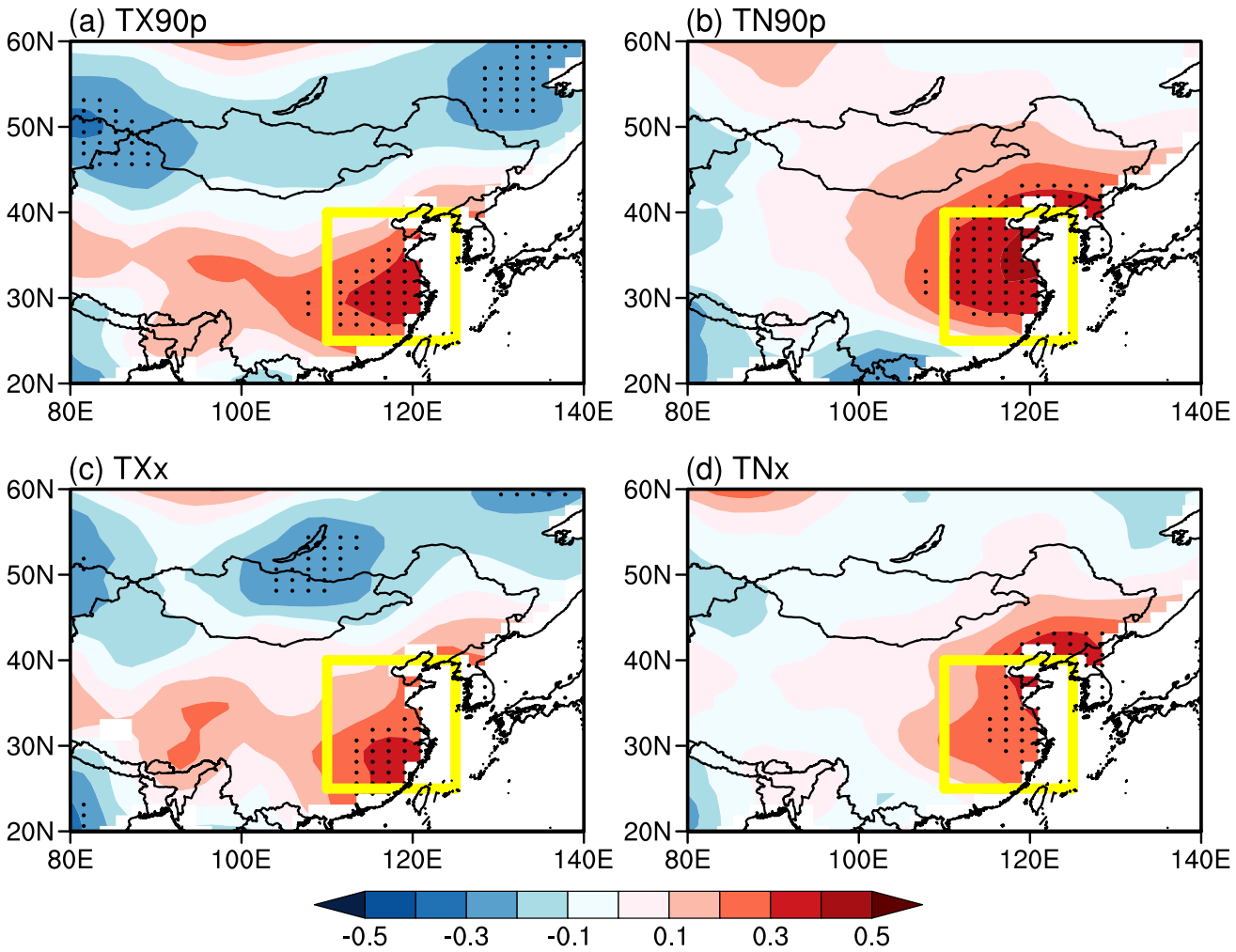

Fig. 1 Correlation maps between the summer NAO and extreme temperature indices in East Asia. **a** TX90p. **b** TN90p. **c** TXx. **d** TNx. Dotted areas indicate significant values at the 95% confidence level based on the Student *t*-test. The yellow boxes represent the CEC

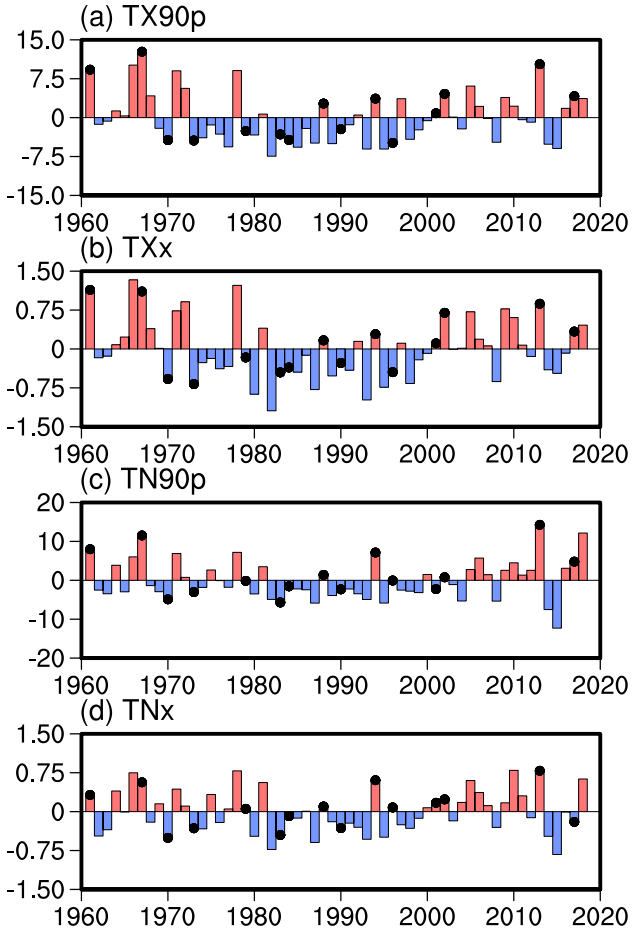

Fig. 2 Time series of the summer area-averaged **a** TX90p (%), **b** TXx (°C), **c** TN90p (%) and **d** TNx (°C) in the CEC (25°–40°N, 110°–125°E). The black dots represent the occurrences of pNAO

amplifying the effect of pNAO on strengthening the extreme heat events in the CEC, in other words, there may be a synergistic effect of pNAO and another factor.

Firstly, we want to know whether there is difference between the pNAO strength in the years with strong (red bars with black dots in Fig. 2a or b) and weak (blue bars with black dots in Fig. 2a or 2b) extreme heat events. The pNAO years with strong and weak extreme heat events are also shown in Table S1. Figure 3a shows the NAO anomalies for the pNAO years with strong and weak extreme heat events, and the difference between them. It is obvious that the strength of the pNAO in the strong extreme heat events years is much greater than that in the weak extreme heat events years, and the difference between them is significant at the 95% confidence level based on the Student *t*-test. This result implies that the extreme heat events in the CEC have a stronger response to a strengthened pNAO. Next, we aim to explore the factors leading to an increased extreme heat events response in the CEC. Figure 3b shows the composite difference of the SSTA between the pNAO years with strong and weak extreme heat events. It is clear that there is a large area exhibiting significantly positive anomaly over the NWP, which means that there is a stronger pNWP SSTA in the pNAO years with strong extreme heat events in the CEC. We further select the domain (20°–40°N, 130°–180°E) to quantify the NWP SST variation, and Fig. 3c further displays the NWP SSTA for the different pNAO years with strong and weak extreme heat events and the difference between them. It can be clearly seen that there is a strong pNWP SSTA in the pNAO years with strong extreme heat events. However, as for the years with weak extreme heat events, there is not such a significantly positive SSTA over the NWP. The

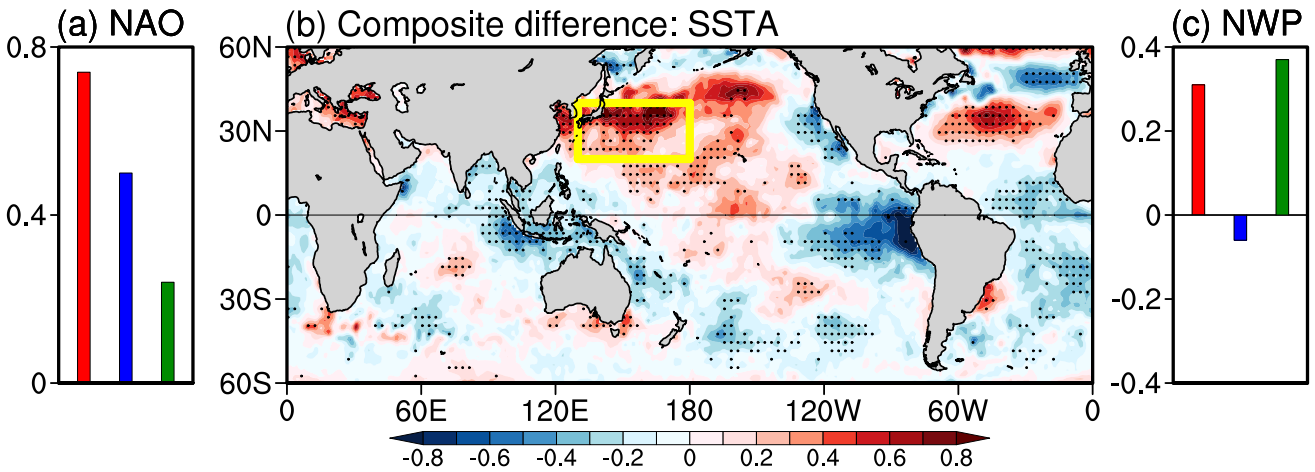

Fig. 3 **a** The NAO anomalies for the pNAO years with strong (the red bar) and weak (the blue bar) extreme heat events, and the green bar represents the difference between them. **b** Composite difference of the SSTA (°C) between the pNAO years with strengthened and weakened extreme heat events. Dotted areas indicate significant values at the 95% confidence level based on the Student *t* test. The yellow box represents the NWP. **c** As in (**a**), but for the NWP SSTA (°C)

difference between the them is also significant at the 95% confidence level based on the Student *t*-test. The above results imply that it could be the pNWP SSTA that leads to a stronger pNAO strength, which further yields a stronger extreme heat event response in the CEC.

Figure 4 further shows the correlation maps between the summer global SSTA and area-averaged extreme temperature indices in the CEC. There are many large areas showing significant correlation with the extreme temperature indices, including the NWP. The significantly correlated area in the NWP is relatively stable for different extreme heat indices, and the NWP is close to the research area and may have adjacent effect on the extreme heat events in the CEC. The NWP SST is positively correlated to the TN90p and TX90p in Fig. 4a and b, which implies that the occurrence of warm NWP SST is likely to be accompanied by the increased extreme heat event frequency (Huang et al. 2010). And the positive correlation between the NWP SST and TXx (TNx) in Fig. 4c, d indicates that the daily temperature is higher than normal when the NWP gets warmer. The above results in Figs. 3 and 4 imply that the NWP SSTA could be another important factor influencing the variation of extreme heat events in the CEC.

Based on the above results, the pNAO and pNWP SSTA are both related to the increased extreme heat events in CEC. Therefore, we further investigated the combined effect of these two factors on the summer extreme heat events in the CEC. To include more cases in this study, we use 0.6 standard deviations to determine the occurrence of the pNAO or pNWP SSTA event. Table 2 lists the numbers and years of the joint events of the summer pNAO and summer pNWP SSTA (pNAO ⊕ pNWP), single summer pNAO events and single summer pNWP SSTA events. As is shown in the Table 2, there are 24 cases in total. Among the 24 cases, 6 cases are the joint events summer pNAO ⊕ pNWP, 9 cases are the single summer pNAO events, and the rest 9 cases are single summer pNWP SSTA events.

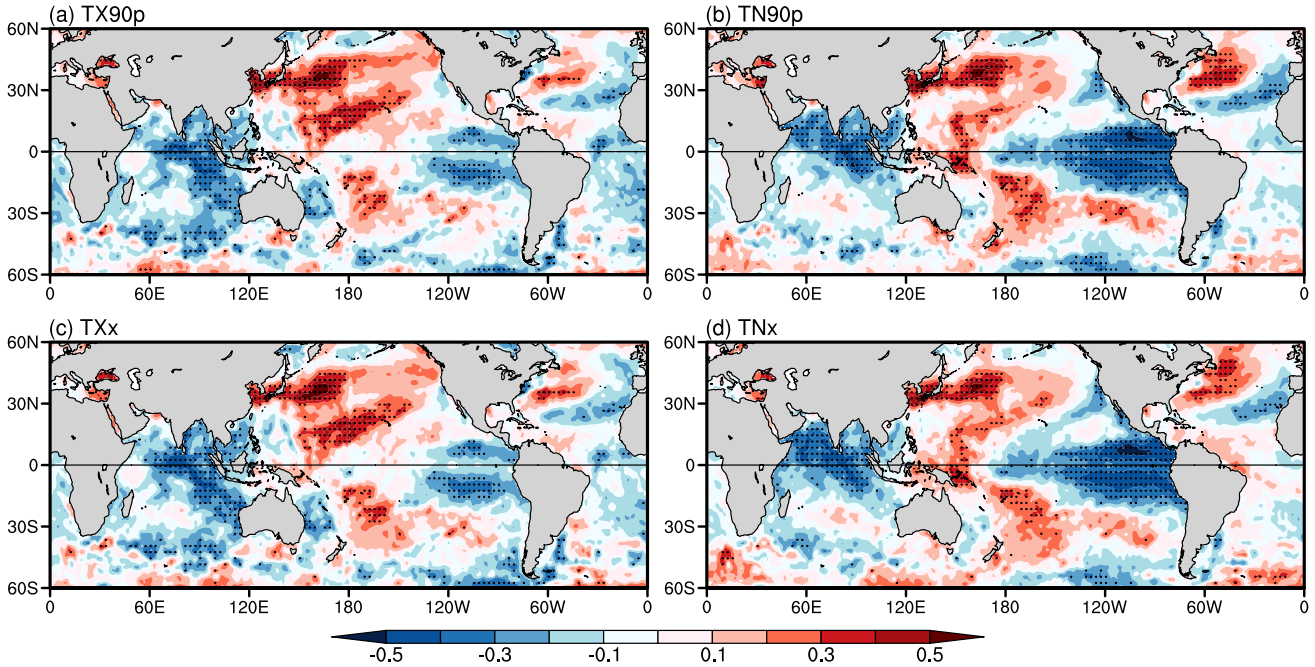

Fig. 4 Correlation maps between the summer global SSTA and area-averaged extreme temperature indices in the CEC (25°–40°N, 110°–125°E). **a** TX90p **b**. TN90p. **c** TXx. **d** TNx. Dotted areas indicate significant values at the 95% confidence level based on the Student t-test

Table 2 Numbers and years of the joint events of summer pNAO and pNWP SSTA (pNAO ⊕ pNWP), single summer pNAO events and single summer pNWP SSTA events

	Joint events of summer pNAO and summer pNWP (pNAO ⊕ pNWP)	Single summer pNAO events	Single summer pNWP SSTA events
Numbers	6	9	9
Years	1961, 1967, 1994, 2001, 2013, 2017	1970, 1973, 1979, 1983, 1984, 1988, 1990, 1996, 2002	1964, 1971, 1975, 1978, 1991, 1998, 1999, 2000, 2004

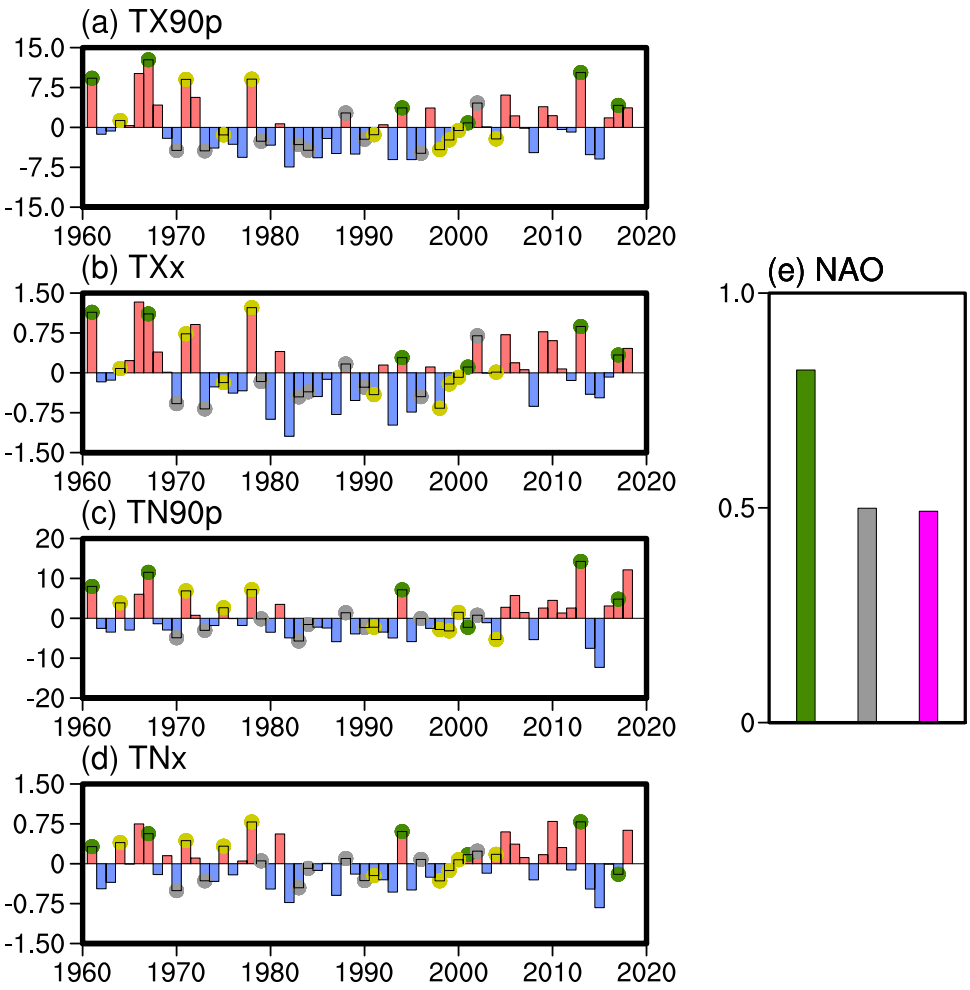

Fig. 5 Time series of the summer area-averaged **a** TX90p (%), **b** TXx (°C), **c** TN90p (%) and **d** TNx (°C) in the CEC (25°–40°N, 110°–125°E). The green, grey and yellow dots represent the joint events of summer pNAO and pNWP SSTA (pNAO ⊕ pNWP), single summer pNAO events and single summer pNWP SSTA events respectively. **e** The NAO anomalies for the joint events summer pNAO ⊕ pNWP (green), single summer pNAO events (grey) and joint events years after removing the NWP signal (magenta), respectively

After dividing into different kinds of cases, the three greatest TX90p anomalies in Fig. 5a are all joint events summer pNAO ⊕ pNWP, which implies there are greater extreme heat index magnitudes for joint events summer pNAO ⊕ pNWP. Besides, all the joint events summer pNAO ⊕ pNWP are positive TX90p or TXx anomalies, which demonstrates that the same-sign rate of joint events summer pNAO ⊕ pNWP is far greater that of the other two kinds of single events. Similar results could be found in TN90p and TNx, 5 in 6 joint events summer pNAO ⊕ pNWP are positive, and the only left are weak negative. This result indicates a greater probability of strengthened extreme heat events when the two factors both happen. The averaged TX90p, TXx, TN90p and TNx anomaly values for joint events summer pNAO ⊕ pNWP are 6.83, 0.66, 7.24 and 0.38 respectively, which are much larger (up to 10 times) than those for the single summer pNAO events (–2.07, –0.23, –1.72 and –0.13) and single summer pNWP SSTA events (0.81, 0.06, 0.94 and 0.17). It is shown in Fig. 3a that there are greatly strengthened extreme heat events when pNAO is stronger. To further confirm whether the stronger pNAO happens in the joint events summer pNAO ⊕ pNWP, we compare the NAO anomalies for different events in Fig. 5e. It is clear that the NAO shows a much greater positive anomaly in the joint events summer pNAO ⊕ pNWP than that in the single summer pNAO events. Besides, after removing the NWP signal from the time series of the NAO index by the linear regression, the positive pNAO anomaly in the joint events years is much smaller. This result implies that pNWP SST could strengthen the pNAO, which means that pNWP SST is favorable for a greater pNAO anomaly. The above results manifest that there is a strong synergistic effect of the summer pNAO and pNWP SSTA, and the cooccurrence of the two factors leads to a higher daily temperature and increased hot day frequency. In other words, there will be more likely to be strengthened extreme heat events in the CEC when both of the two factors occur.

Figure 6 further shows the composite maps of summer extreme temperature indices for different events. In the joint events summer pNAO ⊕ pNWP (Fig. 6a, d, g and j), we can clearly see that the extreme heat indices exhibit significantly positive anomalies in the CEC, and the area with the synergistic effect of the summer pNAO and pNWP SSTA could cover 20° to 40 °N, 90 °E to the eastern China. Although

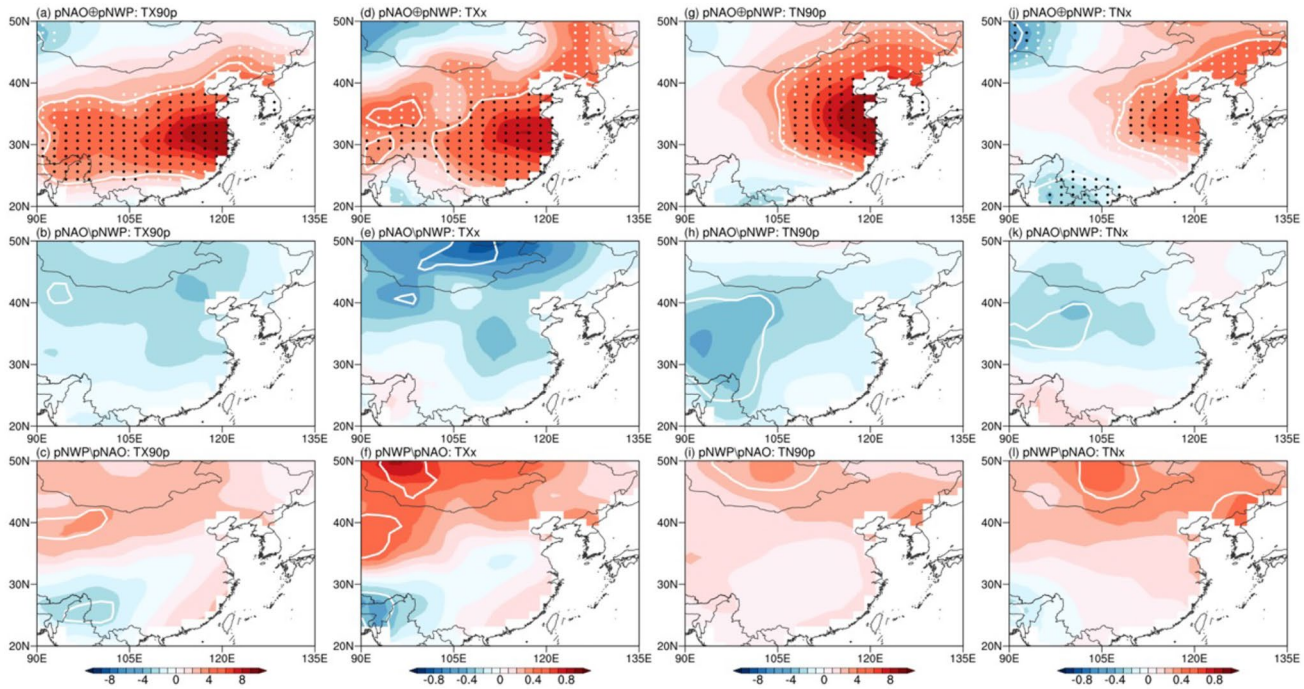

Fig. 6 Composite maps of summer extreme temperature indices for different events. From the left to right columns: TX90p, TXx, TN90p and TNx. From the top to bottom rows: joint events summer pNAO ⊕ pNWP, single summer pNAO events and single summer pNWP SSTA events. The dotted areas indicate the synergistic effect of summer pNAO and pNWP SSTA, and the black dotted areas indicate the synergistic effect is significant at the 90% confidence level based on the bootstrapping method. The white contour lines indicate significant values at the 95% confidence level based on the Student *t* test

there may be some different mechanisms which works for TXx and TNx (Lobell et al. 2007; Yeh et al. 2021), the synergistic effect for the four indices is all evident in the CEC, which further highlights the robustness of the synergistic effect on the extreme heat events. It is also worth noting that the synergistic effect of the two factors is significant in most region of the CEC based on the bootstrapping method. The center of the positive anomaly lies in the eastern China, and extends to the central China, covering the region which the NAO is significantly correlated with. However, the anomalous extreme heat events in the CEC for the single summer pNAO events and summer pNWP SSTA events are insignificant (the second and third rows in Fig. 6). By comparing the spatial patterns of the extreme heat indices anomalies in the joint events summer pNAO⊕pNWP with those in the single summer pNAO events and summer pNWP SSTA events, we can clearly see that there is a significant synergistic effect of the summer pNAO and pNWP SSTA on strengthening the extreme heat events in the CEC.

The above results show that there is a significant synergistic effect of the summer pNAO and pNWP SSTA on strengthening the extreme heat events in the CEC, and a stronger pNAO will happen if the pNWP SSTA occurs. Thus, questions are raised: does the synergistic effect arise from the strengthening of the pNAO in the joint events summer pNAO⊕pNWP, and what role does the pNWP SSTA play in the strengthening of the pNAO in the joint events summer pNAO⊕pNWP?

4 The atmospheric circulations in different events

To further determine the difference of the atmospheric circulations between three kinds of events, Fig. 7a, b and c show the composite maps of the summer 500-hPa geopotential height and 850-hPa winds in the East Asia for different events. As shown in Fig. 7a, there is a strong anomalous anticyclone over the eastern China, with strong southerlies in the CEC, and the center of the anticyclone locates between the Shandong Peninsular and Korean Peninsula. The anomalous southerlies in the west side of the anticyclone bring the warm air to the CEC, which is favorable for the increase of air temperature. Besides, the anomalous anticyclone can also hider the southern movement of the cold air to the CEC from the northern area. However, for the single summer pNAO events and single summer pNWP SSTA events, there is not significant

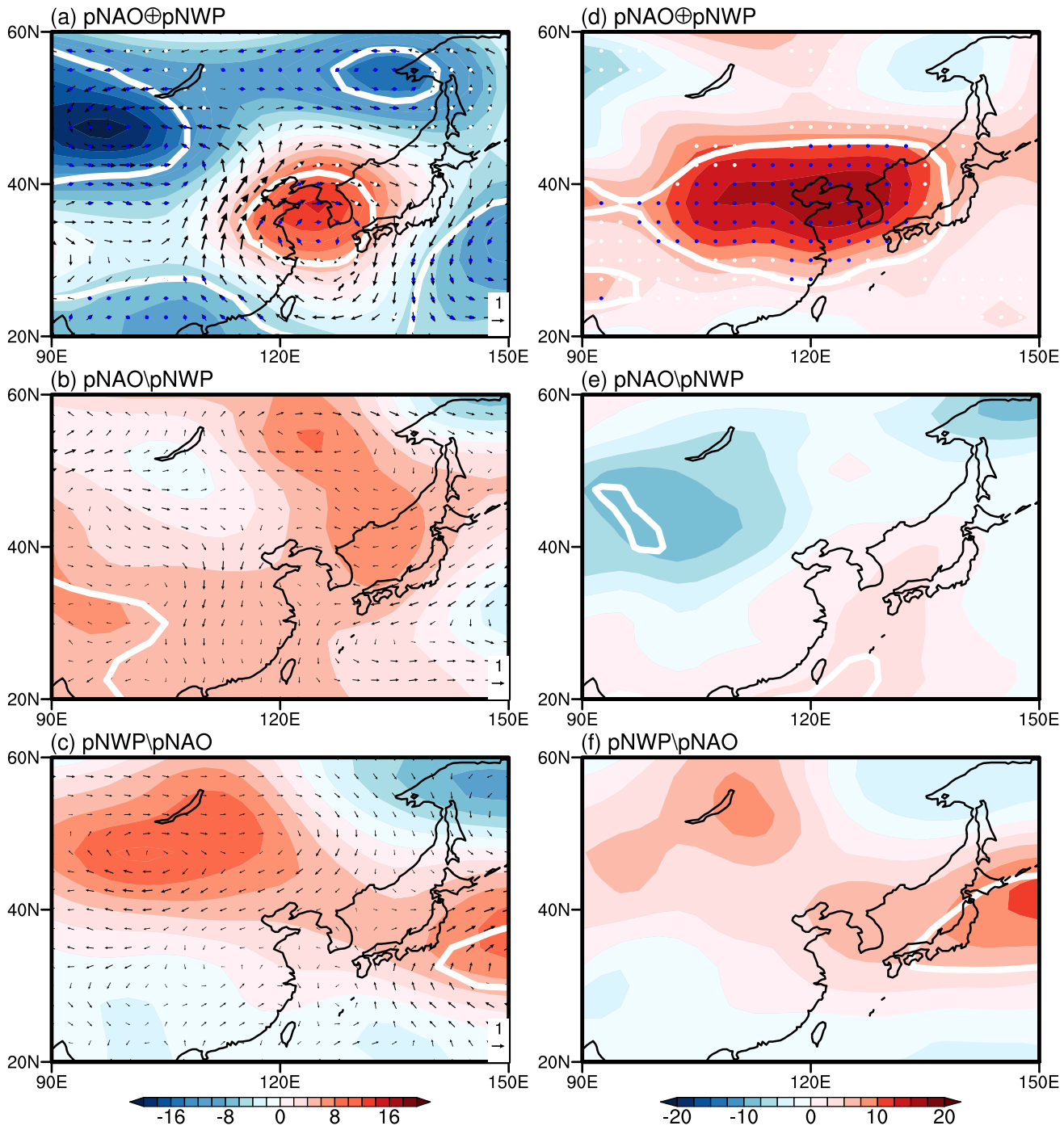

Fig. 7 Composite maps of the summer 500-hPa geopotential height (gpm; shaded) and 850-hPa winds (m s^{-1}; vectors) in the East Asia for (**a**) the joint events of summer pNAO and summer pNWP SSTA (pNAO ⊕ pNWP), **b** single summer pNAO events and **c** single summer pNWP SSTA events. **d**, **e**, **f** As in **a**, **b**, **c**, but for the summer 500 − 1000 hPa atmosphere thickness. The dotted areas in (**a**) and (**d**) indicate the synergistic effect of summer pNAO and summer pNWP SSTA, and the blue dotted areas indicate the synergistic effect is significant at the 90% confidence level based on the bootstrapping method. The white contour lines indicate significant values at the 95% confidence level based on the Student *t* test

atmospheric circulation anomaly over most of the East Asia (Fig. 7b and c). It is worth noting that the two factors show a significant synergistic effect on the anomalous anticyclone in East Asia (Fig. 7a), which means the two factors may influence the extreme heat events by acting synergistically on the atmospheric circulation in the joint events summer pNAO ⊕ pNWP.

According to the previous study (Li et al. 2021), the atmosphere thickness is vital to the air temperature change, and the change of atmosphere thickness comes from the aforementioned perturbation of the upper-level atmospheric circulation, thus we further compare the atmosphere thickness in three kinds of events. Figure 7d, e and f display the composite maps of the summer 500 – 1000 hPa atmosphere thickness in the East Asia for different events. It is clear that there is a large area showing a positive atmosphere thickness anomaly in the CEC, and the two factors have a significant synergistic effect of the increased atmosphere thickness, which means that the positive atmosphere thickness anomaly is much stronger when both of the summer pNAO and pNWP SSTA occur (Fig. 7d). The correlation coefficient between the atmospheric thickness and air temperature over the CEC is 0.74, while the correlation coefficients between the air temperature and TXx, TNx, TX90p and TN90p are 0.68, 0.74, 0.71 and 0.74, respectively, and they are all statistically significant at the 99% confidence level based on the Student t-test. This result implies that the significantly increased atmosphere thickness leads to the air temperature increase in the atmospheric layer (Li et al. 2021), which further favors the extreme heat events in the CEC. However, there is not significant atmosphere thickness anomaly over the CEC during the single summer pNAO events or single summer pNWP SSTA events (Fig. 7e and f).

By comparing different events in Fig. 7, it can be found that the anomalous anticyclone with the significantly positive atmosphere thickness anomaly occurs over the CEC in the joint events summer pNAO ⊕ pNWP. The positive atmosphere thickness anomaly in the joint events summer pNAO ⊕ pNWP is much greater than that in the two kinds of single events, leading to the higher air temperature of the atmosphere layer in the joint events summer pNAO ⊕ pNWP. Therefore, the extreme heat events are far stronger in the joint events summer pNAO ⊕ pNWP, and the CEC is more likely to experience a hot summer.

5 The mechanism of the synergistic effect

The above results show that the summer pNAO and pNWP SSTA have a synergistic effect on the atmospheric circulation over the East Asia, and the significantly increased atmosphere thickness over the CEC contributes to the strengthened extreme heat events. Why is there such a great difference in the atmospheric circulation over East Asia between the joint events summer pNAO ⊕ pNWP and two kinds of single events? We mean to explore this question in this section.

To compare the Rossby wave propagation in different events, T–N wave activity flux is used, and it is a useful way to check the propagation of Rossby wave (Takaya and Nakamura 2001). Figure 8 shows the composite map of summer 500-hPa T-N wave activity flux and anomalous QG stream function for the joint events summer pNAO ⊕ pNWP, single summer pNAO events and all summer pNWP SSTA events. Previous studies have shown that the NAO is able to influence the atmospheric circulation in East Asia via Rossby wave (Watanabe 2004; Chen et al. 2005; Zuo et al. 2015; Li and Ruan 2018), and we further compare the difference of Rossby wave propagation in different events. As shown in Fig. 8a, it is clear that there is obvious easterly propagating Rossby wave from the Atlantic to the East Asia, and the easterly propagation of the Rossby wave is strong over the whole Eurasian continent. Therefore, it can lead to a strong atmospheric circulation response in the East Asia. Although there is easterly Rossby wave propagation from the Atlantic in the single summer pNAO events, the easterly Rossby wave propagation over the east side of the Eurasian continent is quite weak, which denotes the atmospheric circulation response in the East Asia is much weaker in the single summer pNAO events (Fig. 8b). The results in Fig. 5e indicate that the NAO has a much stronger positive anomaly when the pNWP SSTA occurs. Thus, a stronger pNAO leads to the enhanced Rossby wave propagation in the joint events summer pNAO ⊕ pNWP, and results in the significant atmospheric circulation response in the East Asia. How does the pNWP SSTA influence the strength of pNAO? As is shown in Fig. 8c, there is obvious easterly propagating Rossby wave from the western Pacific to the Atlantic in all the pNWP SSTA events, which indicates that pNWP SSTA may influence the atmospheric circulation over the Atlantic, and further lead to a pNAO-like atmospheric response, which can increase the pNAO strength. The above results show that, the pNWP SSTA could lead to a strengthened pNAO via the easterly propagating Rossby wave from the western Pacific, and the resultant stronger pNAO in the joint events summer pNAO ⊕ pNWP may lead to a stronger easterly Rossby wave propagation over the Eurasian continent. Thus, there is a significantly atmospheric circulation response over East Asia in the joint events summer pNAO ⊕ pNWP (Fig. 7a and 8a).

To further confirm the change of Rossby wave propagation from the Atlantic, the Rossby wave ray is compared (Li and Li 2012; Li et al. 2015, 2019b, 2021; and Zhao et al. 2015, 2019). Figure 9 shows the summer stationary Rossby wave trajectories in the horizontally nonuniform flow for different events. As shown in Fig. 9a and b, there is more Rossby wave energy propagating towards the east side of the Eurasian continent, and the Rossby wave is more concentrated over the CEC in the joint events summer pNAO ⊕ pNWP when the wave source is set around the southern activity center of the NAO (35°–45°N, 45°–70°W). The similar result can be found in Fig. 9c and d, which also demonstrates that there is much more

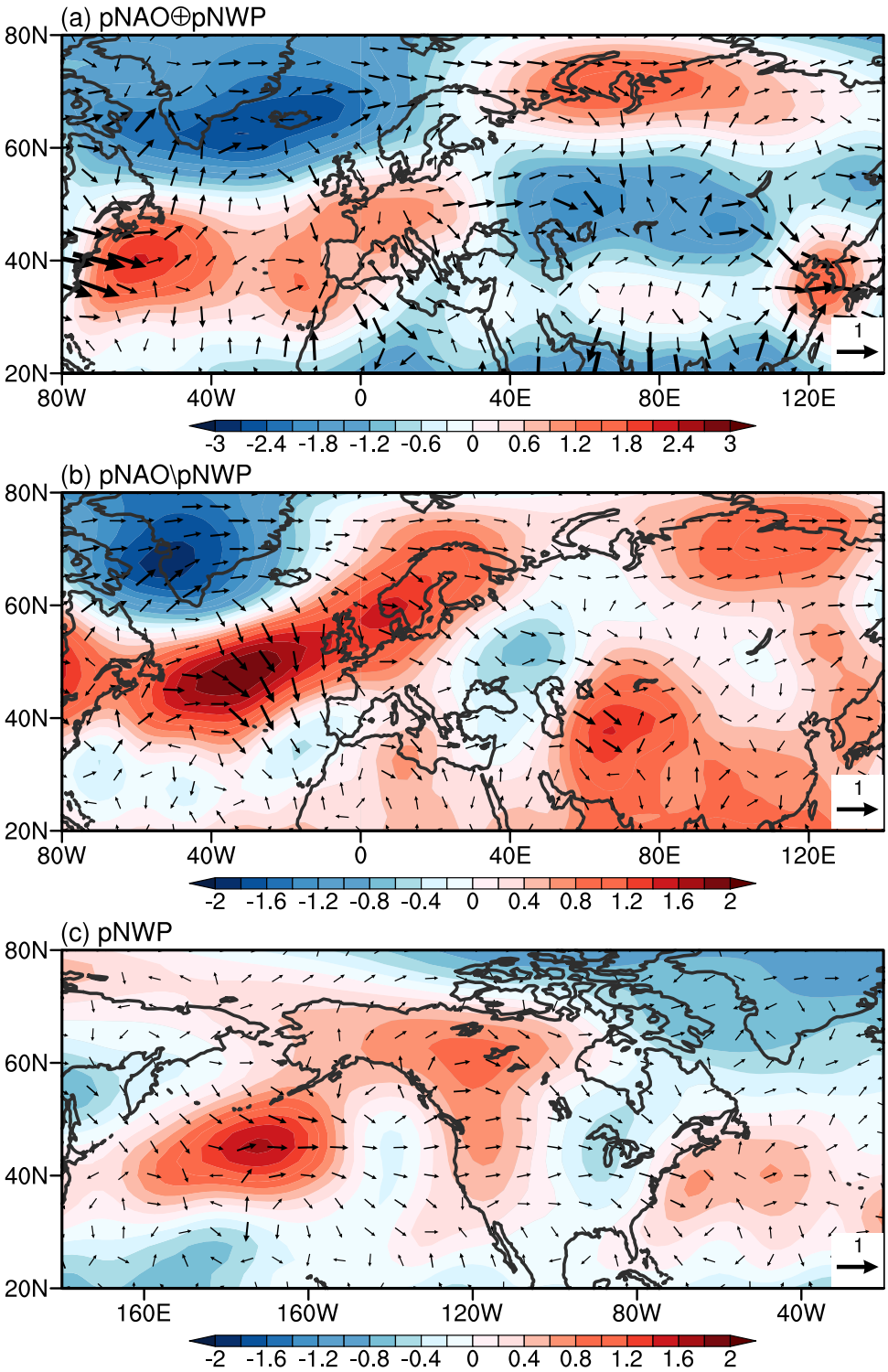

Fig. 8 The composite map of summer 500-hPa T-N wave activity flux ($m^2\ s^{-2}$; vectors) and anomalous QG stream function ($10^6\ m^2\ s^{-1}$; shaded) for (**a**) the joint events of summer pNAO and summer pNWP SSTA (pNAO ⊕ pNWP), **b** single summer pNAO events and **c** all summer pNWP SSTA events

easterly propagating Rossby wave energy in the east side of the Eurasian continent when the wave source is set around the northern activity center of the NAO (55°–65°N, 10°–50°W). The above results further confirm the finding in the results of T–N wave activity flux, which is that there is more Rossby wave propagating easterly over the Eurasian continent, leading to a stronger atmospheric circulation response over the east side of the Eurasian continent in the joint events summer pNAO ⊕ pNWP.

To further confirm the influence of the pNWP SSTA on the pNAO, we further use the LBM and carry three experiments. In the first experiment (EXP1), the heating source

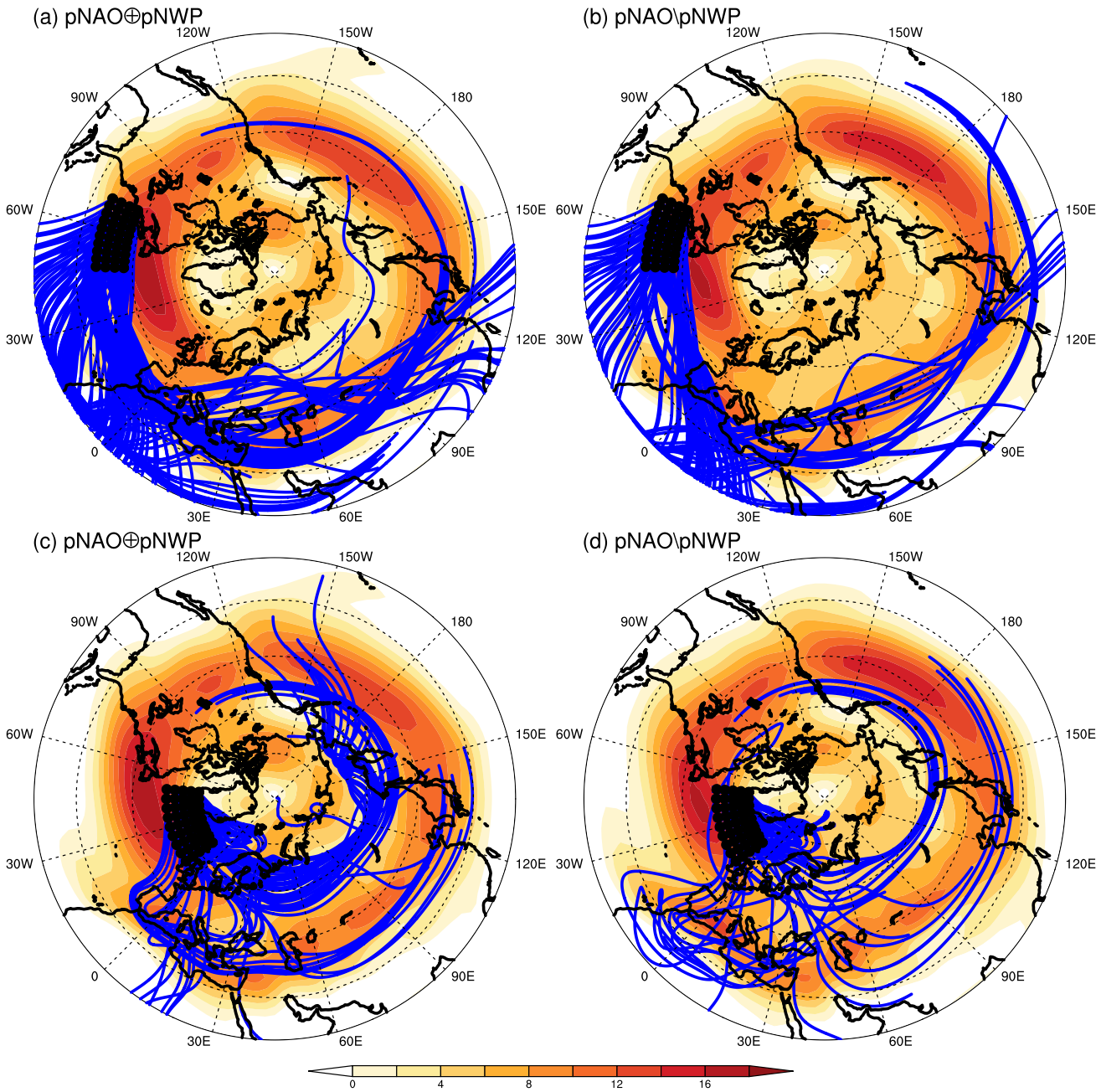

Fig. 9 Summer stationary Rossby wave trajectories in the horizontally nonuniform flow (blue curves) with zonal wavenumber $k=4$ for **a** and **c** the joint events of summer pNAO and summer pNWP SSTA (pNAO ⊕ pNWP), **b** and **d** single summer pNAO events. The black dots denote the Rossby wave source which is set in the southern activity center of NAO in **a** and **b**, and northern activity center of NAO in **c** and **d**. The shaded area is the climatological mean 500 hPa zonal wind (m s^{-1}). The Rossby wave ray tracing is calculated by adopting the approach by Li and Li (2012), Li et al. (2015; 2019b; 2021) and Zhao et al. (2015)

is set in the domain 30°–50°N, 0°–60°W with a 4 K day^{-1} heating peaking at 0.7 sigma level, and the heating sink is set in the domain 60°–80°N, 0°–60°W with a − 6 K day^{-1} heating peaking at 0.6 sigma level, which mimics the pNAO situation. In the second experiment (EXP2), the heating source is set in the domain 20°–40°N, 130°–180°E with a 4 K day^{-1} heating peaking at 0.4 sigma level, which mimics the heating effect of the pNWP SSTA. The third experiment (EXP3) is a combination of EXP1 and EXP2, which includes all the heating effects of pNAO and pNWP. Figure 10 shows the steady 500 hPa geopotential height response in the three experiments. As shown in Fig. 10a, there is a positive geopotential height anomaly response over the CEC, indicating that the NAO is able to influence the atmospheric circulation

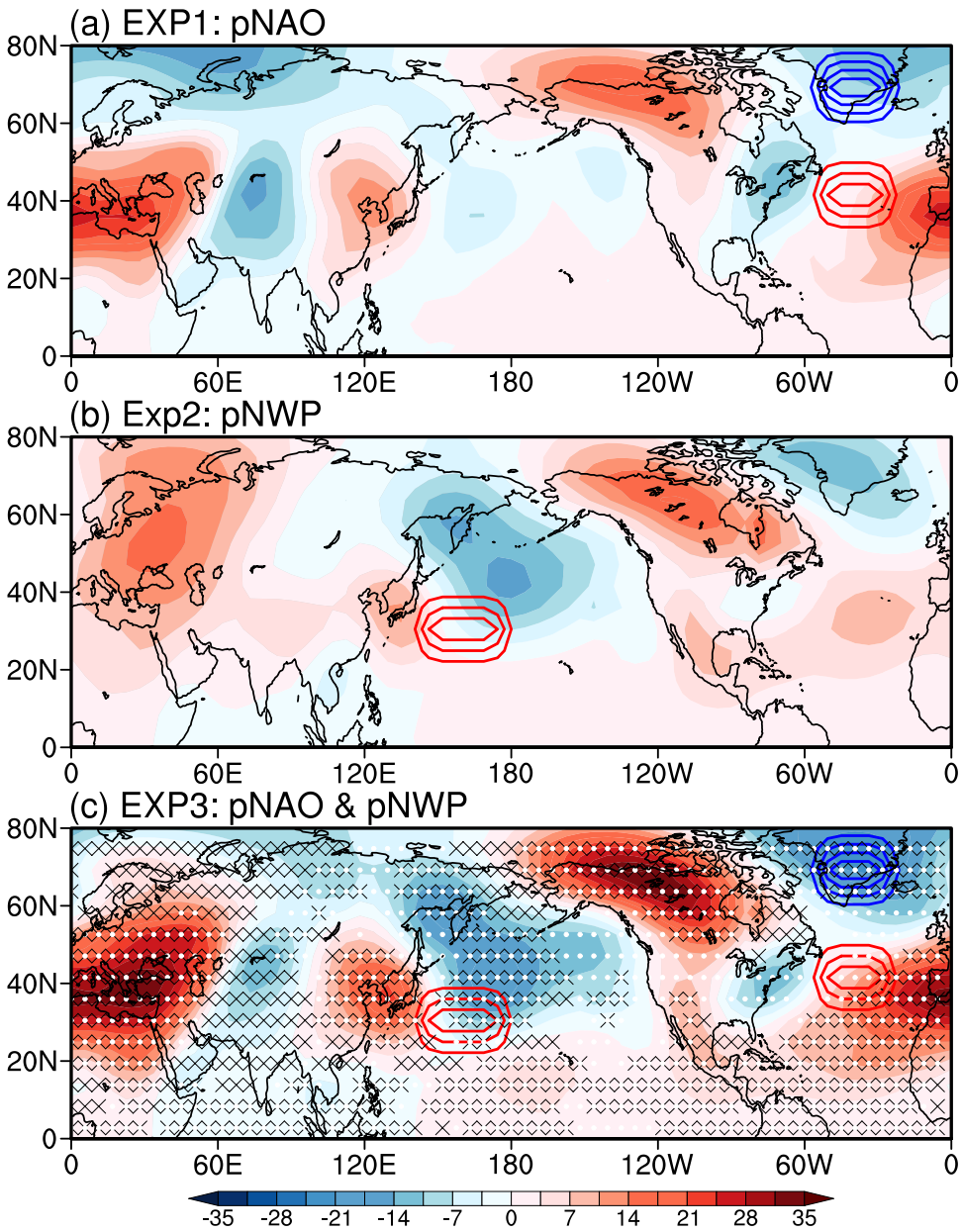

Fig. 10 Steady 500-hPa geopotential height response (gpm) to **a** the NAO, **b** NWP and **c** both of the NAO and NWP heating in the LBM. The red and blue contours (unit: K day^{-1}, contour interval: 1 K day^{-1}) indicate the heating source and heating sink respectively. The black crossed areas indicate the composite differences between EXP3 and EXP1, as well as EXP3 and EXP2, are both significant at the 95% confidence level based on the Student *t* test. The white dotted areas in **c** indicate the synergistic effect of the NAO and NWP heating effect

and induce an anomalous anticyclone in this area. This result is consistent with the T–N wave activity flux and Rossby wave ray results. As shown in Fig. 10b, the heating effect of the NWP can induce the pNAO-like atmospheric response over the Atlantic, which means that the pNAO is likely to be strengthened when the pNWP SSTA occurs. This result may explain why the NAO shows greater positive anomaly in the joint events summer pNAO ⊕ pNWP than that in the single summer pNAO events (Fig. 5e). The pNAO-like atmospheric response to the heating effect over the NWP also confirms the T-N wave activity flux result of all the pNWP SSTA events (Fig. 8c). Besides, there is also a positive geopotential height anomaly response to the heating over the NWP in the CEC, which denotes that the pNWP SSTA has adjacent effect to the atmospheric circulation in the CEC, and it also favors the increase of geopotential height in the CEC (Fig. 10b). It is clear that both the heating effects of pNAO and pNWP could lead to a stronger positive anomalous geopotential height response over the eastern China, which highlights the synergistic effect of the two factors (Fig. 10c). The above LBM results confirm the effects of the pNAO and pNWP SSTA on the atmospheric circulation over the CEC and the effect of the pNWP SSTA on strengthening the pNAO. Thus, the NAO has a greater positive anomaly and a stronger atmospheric circulation response occurs over the CEC in the joint events summer pNAO ⊕ pNWP.

6 Summary and discussion

In this paper, we investigate the synergistic effect of the summer pNAO and pNWP SSTA on the extreme heat events in the CEC, and find that the extreme heat events are significantly strengthened when the two factors occur, which means the cooccurrence of the two factors may lead the CEC to experience a hot summer.

Figure 11 shows the process of the synergistic effect of the summer pNAO and pNWP SSTA on the extreme heat events in the CEC. The summer pNWP SSTA may increase the strength of summer pNAO via the atmospheric bridge, leading to a strengthened summer pNAO. There is eastward propagating Rossby wave from the western Pacific to the Atlantic, and the LBM confirms that the heating effect over the NWP can induce a pNAO-like atmospheric response over the Atlantic. Thus, there is a stronger summer pNAO. And the summer pNAO may influence the atmospheric circulation around the CEC via another atmospheric bridge which is the eastward propagating Rossby wave from the Atlantic. As the pNAO is much stronger when the pNWP SSTA occurs, the Rossby wave propagation over the Eurasian continent is stronger in the joint events summer pNAO ⊕ pNWP, which induces an anomalous anticyclone in the eastern China. The southerlies in the west side of the anomalous anticyclone bring the warm air to the CEC, and the significantly increased atmosphere thickness in the CEC induces the increase in the air temperature of the atmospheric layer, which favors the strengthened extreme heat events in the CEC. Besides, the pNWP SSTA also has adjacent effect on the atmospheric circulation over the CEC, there is a positive geopotential height anomaly response over the CEC to the heating effect over the NWP. Therefore, the summer pNAO and pNWP SSTA have a synergistic effect on the extreme heat events in the CEC, and the summer extreme heat events are significantly strengthened.

There are strong extreme heat events in China during the 2022 summer, and many regions in China suffer record-breaking high temperature. It is worth noting that there are also the pNAO and pNWP SSTA happening in the summer of 2022 (figures not shown), which indicates that the extreme heat events in China may be partially resulted by the synergistic effect of the two factors, and it is of vital importance to pay more attention to the synergistic effect of the two factors in the weather forecast. However, besides the CEC, the western part of China also suffers extreme heat events in 2022 summer, especially for the Sichuan and Chongqing, and these areas are out of our investigated area. This implies that there may be other factors also contributing to the 2022 summer extreme heat events in China, especially in the western China, although the summer pNAO and

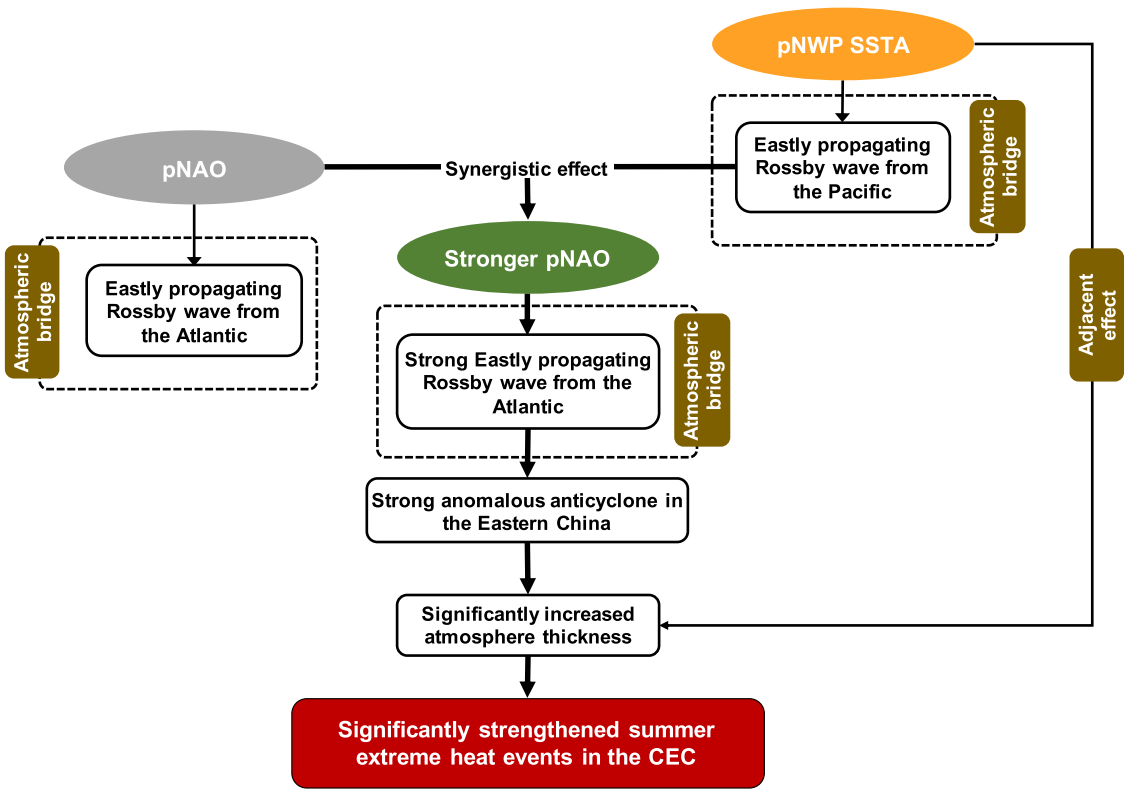

Fig. 11 The schematic diagram showing the synergistic effect of the summer pNAO and pNWP SSTA on the extreme heat events in the CEC

pNWP SSTA have important influence on the extreme heat events in the CEC. More detailed instigations of the 2022 summer extreme heat events in China are needed.

Here, we only show the result based on 0.6 standards deviations. However, the synergistic effect of summer pNAO and pNWP SSTA is also evident under other thresholds, which highlights the robustness of the synergistic effect (Fig. S1). Besides, the greater the threshold is, the stronger the synergistic effect will be. However, a relatively great threshold could lead to relatively small sample sizes. Thus, we use the threshold of 0.6 standard deviations in the manuscript. It is also worth noting that we only discuss the synergistic effect of the summer pNAO and pNWP SSTA, there might be other factors having synergistic effect with the two factors. Besides the NWP, there are other places showing significant correlation with the extreme heat events in the CEC (Fig. 4), and they may also have the potential to influence the extreme heat events in the CEC synergistically, which needs further research. There are also some places in Fig. 3b which shows significant difference in different pNAO years with strong and weak extreme heat events, implying that they may contribute to the change in the response of the extreme heat events in the CEC, and they may also lead to a synergistic effect, which needs more detailed research. Furthermore, the synergistic effect of multiple factors is also worth investigating, but it requires the data covering a much longer time period to provide enough sample sizes.

Supplementary Information The online version contains supplementary material available at https://doi.org/10.1007/s00382-023-06807-6.

Acknowledgements We thank all the data providers. This work is supported by the National Natural Science Foundation of China (NSFC) Project (42288101), Laoshan Laboratory (No.LSKJ202202600), and Shandong Natural Science Foundation Project (ZR2019ZD12). We are thankful to Center for High Performance Computing and System Simulation, Pilot National Laboratory for Marine Science and Technology (Qingdao) for providing computing resource. We are thankful to the three anonymous reviewers.

Author contributions HW, JL and FZ contributed to the study conception and design. Material preparation, data collection and analysis were performed by HW and FL. The first draft of the manuscript was written by HW, and all authors commented on previous versions of the manuscript and helped revise the manuscript. All authors read and approved the final manuscript.

Funding This work is supported by the National Natural Science Foundation of China (NSFC) Project (42288101), Laoshan Laboratory (No. LSKJ202202600), and Shandong Natural Science Foundation Project (ZR2019ZD12).

Data availability The HadISST1 dataset was obtained from https://www.metoffice.gov.uk/hadobs/hadisst/. The HadEX3 dataset was obtained from https://www.metoffice.gov.uk/hadobs/hadex3/. The NCEP–NCAR reanalysis version 1 dataset was obtained from https://psl.noaa.gov/data/gridded/data.ncep.reanalysis.html. The HadCRUT4 dataset was obtained from https://www.metoffice.gov.uk/hadobs/hadcrut4/.

Declarations

Conflict of interest The authors declare no competing interests.

References

Alessandro AP, de Garín AB (2003) A study on predictability of human physiological strain in Buenos Aires City. Meteorol Appl 10:263–271. https://doi.org/10.1017/S1350482703003062

An XD, Sheng LF, Li JP (2021) Synergistic effect of SST anomalies in the North Pacific and North Atlantic on summer surface air temperature over the Mongolian Plateau. Clim Dyn 56:1449–1465. https://doi.org/10.1007/s00382-020-05541-7

Bastos A, Gouveia CM, Trigo RM, Running SW (2014) Analysing the spatio-temporal impacts of the 2003 and 2010 extreme heatwaves on plant productivity in europe. Biogeosciences 11:3421–3435. https://doi.org/10.5194/bg-11-3421-2014

Black E, Blackburn M, Harrison G, Hoskins B, Methven J (2004) Factors contributing to the summer 2003 European heatwave. Weather 59:217–223. https://doi.org/10.1256/wea.74.04

Chen RD, Lu RY (2015) Comparisons of the circulation anomalies associated with extreme heat in different regions of eastern China. J Clim 28:5830–5844. https://doi.org/10.1175/JCLI-D-14-00818.1

Chen X, Zhou T (2018) Relative contributions of external SST forcing and internal atmospheric variability to July–August heat waves over the Yangtze River valley. Clim Dyn 51(11–12):4403–4419. https://doi.org/10.1007/s00382-017-3871-y

Chen W, Yang S, Huang R (2005) Relationship between stationary planetary wave activity and the East Asian winter monsoon. J Geophys Res Atmos 110:D14. https://doi.org/10.1029/2004JD005669

Chen RD, Wen ZP, Lu RY (2016) Evolutions of the circulation anomalies and the quasi-biweekly oscillations associated with extreme heat events in South China. J Clim 29:6909–6921. https://doi.org/10.1175/JCLI-D-16-0160.1

Deng K, Ting M, Yang S, Tan Y (2018) Increased frequency of summer extreme heat waves over Texas area tied to the amplification of Pacific zonal SST gradient. J Clim 31:5629–5647. https://doi.org/10.1175/JCLI-D-17-0554.1

Deser C, Simpson IR, McKinnon KA, Phillips AS (2017) The northern hemisphere extratropical atmospheric circulation response to ENSO: how well do we know it and how do we evaluate models accordingly? J Clim 30:5059–5082. https://doi.org/10.1175/JCLI-D-16-0844.1

Deser C, Simpson IR, Phillips AS, McKinnon KA (2018) How well do we know ENSO's climate impacts over North America, and how do we evaluate models accordingly? J Clim 31:4991–5014. https://doi.org/10.1175/JCLI-D-17-0783.1

Ding T, Ke Z (2015) Characteristics and changes of regional wet and dry heat wave events in China during 1960–2013. Theoret Appl Climatol 122:651–665. https://doi.org/10.1007/s00704-014-1322-9

Dunn RJH, Alexander LV, Donat MG et al (2020) Development of an updated global land in situ-based data set of temperature and precipitation extremes: HadEX3. J Geophys Res Atmos 125:e2019JD032263. https://doi.org/10.1029/2019JD032263

Fragkoulidis G, Wirth V, Bossmann P, Fink A (2018) Linking northern hemisphere temperature extremes to Rossby wave packets. Q J R Meteorol Soc 144:553–566. https://doi.org/10.1002/qj.3228

Frankignoul C, Sennechael N, Kwon Y-O, Alexander MA (2011) Influence of the meridional shifts of the Kuroshio and the Oyashio

Extensions on the atmospheric circulation. J Clim 24:762–777. https://doi.org/10.1175/2010JCLI3731.1

Gershunov A, Cayan DR, Iacobellis SF (2009) The great 2006 heat wave over California and Nevada: signal of an increasing trend. J Clim 22:6181–6203. https://doi.org/10.1175/2009JCLI2465.1

Gong DY, Pan YZ, Wang JA (2004) Changes in extreme daily mean temperatures in summer in eastern China during 1955–2000. Theoret Appl Climatol 77:25–37. https://doi.org/10.1007/s00704-003-0019-2

Horton RM, Mankin JS, Lesk C, Coffel E, Raymond C (2016) A review of recent advances in research on extreme heat events. Curr Clim Change Rep 2:242–259. https://doi.org/10.1007/s40641-016-0042-x

Hoskins BJ, Karoly DJ (1981) The steady linear response of a spherical atmosphere to thermal and orographic forcing. J Atmos Sci 38:1179–1196. https://doi.org/10.1175/1520-0469(1981)038%3c1179:TSLROA%3e2.0.CO;2

Hu KM, Huang G, Qu X, Huang RH (2012) The Impact of Indian ocean variability on high temperature extremes across south of Yangtze River Valley in late summer. Adv Atmos Sci 29:91–100. https://doi.org/10.1007/s00376-011-0209-2

Huang DQ, Qian YF, Zhu J (2010) Trends of temperature extremes in China and their relationship with global temperature anomalies. Adv Atmos Sci 27(4):937–946. https://doi.org/10.1007/s00376-009-9085-4

Hurrell JW (1995) Decadal trends in the North Atlantic oscillation: regional temperatures and precipitation. Science 269:676. https://doi.org/10.1126/science.269.5224.676

Kalnay E, Kanamitsu M, Kistler R et al (1996) The NCEP/NCAR 40 year reanalysis project. Bull Am Meteorol Soc 77(3):437–471. https://doi.org/10.1175/1520-0477(1996)077%3c0437:TNYRP%3e2.0.CO;2

Karoly DJ (1983) Rossby wave propagation in a barotropic atmosphere. Dyn Atmos Oceans 7:111–125. https://doi.org/10.1016/0377-0265(83)90013-1

Kornhuber K, Osprey S, Coumou D, Petri S, Petoukhov V, Rahmstorf S, Gray L (2019) Extreme weather events in early summer 2018 connected by a recurrent hemispheric wave-7 pattern. Environ Res Lett 14:054002. https://doi.org/10.1088/1748-9326/ab13bf

Li C (2008) Coupling mode analysis of summer precipitation in mid-low valley of Yangtze river and sea surface temperature in northwest Pacific (in Chinese). J Trop Oceanogr 4:38–44

Li YJ, Li JP (2012) Propagation of planetary waves in the horizontal non-uniform basic flow (in Chinese). Chin J Geophys 55:361–371. https://doi.org/10.6038/j.issn.0001-5733.2012.02.001

Li L, Luo T (2014) Intraseasonal oscillation of SST over northwest Pacific and its relationship with summer intraseasonal rainfall in eastern China (in Chinese). Trans Atmos Sci 37:1674–7097

Li L, Nathan TR (1997) Effects of low-frequency tropical forcing on intraseasonal tropical-extratropical interactions. J Atmos Sci 54:332–346. https://doi.org/10.1175/1520-0469(1997)054%3c0332:EOLFTF%3e2.0.CO;2

Li JP, Ruan CQ (2018) The North Atlantic-Eurasian teleconnection in summer and its effects on Eurasian climates. Environ Res Lett 13:024007. https://doi.org/10.1088/1748-9326/aa9d33

Li JP, Wang JXL (2003) A new North Atlantic oscillation index and its variability. Adv Atmos Sci 20:661–676. https://doi.org/10.1007/BF02915394

Li YJ, Li JP, Jin FF, Zhao S (2015) Interhemispheric propagation of stationary Rossby waves in the horizontally nonuniform background flow. J Atmos Sci 72:3233–3256. https://doi.org/10.1175/JAS-D-14-0239.1

Li JP, Zheng F, Sun C, Feng J, Wang J (2019a) Pathways of influence of the Northern Hemisphere mid-high latitudes on East Asian climate: a review. Adv Atmos Sci 36:902–921. https://doi.org/10.1007/s00376-019-8236-5

Li YJ, Feng J, Li JP, Hu AX (2019b) Equatorial windows and barriers for stationary Rossby wave propagation. J Clim 32:6117–6135. https://doi.org/10.1175/JCLI-D-18-0722.1

Li JP, Xie TJ, Tang XX, Wang H, Sun C, Feng J, Zheng F, Ding RQ (2021) Influence of the NAO on wintertime surface air temperature over the East Asia: Multidecadal variability and decadal prediction. Adv Atmos Sci 39:625–642. https://doi.org/10.1007/s00376-021-1075-1

Liu Q, Wen N, Liu Z (2006) An observational study of the impact of the North Pacific SST on the atmosphere. Geophys Res Lett 33:L18611. https://doi.org/10.1029/2006GL026082

Lobell DB, Bonfils C, Duffy PB (2007) Climate change uncertainty for daily minimum and maximum temperatures: a model intercomparison. Geophys Res Lett 34:L05715. https://doi.org/10.1029/2006GL028726

Lu RY, Chen RD (2016) A review of recent studies on extreme heat in China. Atmos Ocean Sci Lett 9:114–121. https://doi.org/10.1080/16742834.2016.1133071

Matsumura S, Horinouchi T, Sugimoto S, Sato T (2016) Response of the Baiu rainband to northwest Pacific SST anomalies and its impact on atmospheric circulation. J Clim 29:3075–3093. https://doi.org/10.1175/JCLI-D-15-0691.1

Meehl GA, Tebaldi C (2004) More intense, more frequent, and longer lasting heat waves in the 21st century. Science 305:994–997. https://doi.org/10.1126/science.1098704

Morice CP, Kennedy JJ, Rayner NA, Jones PD (2012) Quantifying uncertainties in global and regional temperature change using an ensemble of observational estimates: The HadCRUT4 dataset. J Geophys Res 117:D08101. https://doi.org/10.1029/2011JD017187

Peng JB (2014) An investigation of the formation of the heat wave in southern China in summer 2013 and the relevant abnormal subtropical high activities. Atmos Ocean Sci Lett 7:286–290. https://doi.org/10.1080/16742834.2014.11447177

Perkins SE (2015) A review on the scientific understanding of heatwaves-their measurement, driving mechanisms, and changes at the global scale. Atmos Res 164:242–267. https://doi.org/10.1016/j.atmosres.2015.05.014

Rayner NA, Parker DE, Horton EB, Folland CK, Alexander LV, Rowell DP, Kent EC, Kaplan A (2003) Global analyses of sea surface temperature, sea ice, and night marine air temperature since the late nineteenth century. J Geophys Res 108:4407. https://doi.org/10.1029/2002JD002670

Russo S, Sillmann J, Fischer EM (2015) Top ten European heatwaves since 1950 and their occurrence in the coming decades. Environ Res Lett 10:124003. https://doi.org/10.1088/1748-9326/10/12/124003

Sparrow S, Su Q, Tian F, Li S, Chen Y, Chen W, Luo F, Freychet N, Lott FC, Dong B, Tett SFB, Wallom D (2018) Attributing human influence on the July 2017 Chinese heatwave: the influence of sea-surface temperatures. Environ Res Lett 13(11):114004. https://doi.org/10.1088/1748-9326/aae356

Sun J (2012) Possible impact of the summer North Atlantic oscillation on extreme hot events in China. Atmos Oceanic Sci Lett 5:231–234. https://doi.org/10.1080/16742834.2012.11446996

Sun Y, Li JP (2022) Synergistic effect of El Niño and the North Pacific Oscillation on wintertime precipitation over southeastern China and the East China Sea Kuroshio area. Clim Dyn 58:1635–1649. https://doi.org/10.1007/s00382-021-05982-8

Sun J, Wang H, Yuan W (2008) Decadal variations of the relationship between the summer North Atlantic oscillation and middle East Asian air temperature. J Geophys Res 113:D15107. https://doi.org/10.1029/2007JD009626

Sun Y, Zhang X, Zwiers FW, Song L, Wan H, Hu T, Yin H, Ren G (2014) Rapid increase in the risk of extreme summer heat in Eastern China. Nat Clim Change 4:1082–1085. https://doi.org/10.1038/NCLIMATE2410

Takaya K, Nakamura H (2001) A formulation of a phase-independent wave activity flux for stationary and migratory quasi geostrophic eddies on a zonally varying basic flow. J Atmos Sci 58:608–627. https://doi.org/10.1175/1520-0469(2001)058%3c0608:AFOAPI%3e2.0.CO;2

Tan JG, Zheng Y, Song G, Kalkstein LS, Kalkstein AJ, Tang X (2007) Heat wave impacts on mortality in Shanghai, 1998 and 2003. Int J Biometeorol 51:193–200. https://doi.org/10.1007/s00484-006-0058-3

Tang XX, Li JP, Zhang YZ, Li YJ, Zhao S (2022) Synergistic effect of El Niño and negative phase of North Atlantic Oscillation on winter precipitation in the southeastern United States. J Clim. https://doi.org/10.1175/JCLI-D-22-0293.1

Wallace JM, Gutzler D (1981) Teleconnections in the geopotential height field during the Northern Hemisphere winter. Mon Wea Rev 109:784–812. https://doi.org/10.1175/1520-0493(1981)109%3c0784:TITGHF%3e2.0.CO;2

Wang H, Zheng F, Diao YN, Li JP, Sun RP, Tang XX, Sun Y, Li F, Zhang YZ (2022) The synergistic effect of the preceding winter Northern Hemisphere annular mode and spring tropical North Atlantic SST on spring extreme cold events in the mid-high latitudes of East Asia. Clim Dyn 59:3175–3191. https://doi.org/10.1007/s00382-022-06237-w

Watanabe M (2004) Asian jet waveguide and a downstream extension of the North Atlantic Oscillation. J Clim 17:4674–4691. https://doi.org/10.1175/JCLI-3228.1

Whitham G (1960) A note on group velocity. J Fluid Mech 9:347–352. https://doi.org/10.1017/S0022112060001158

Wu Z, Jiang Z, Li J, Zhong S, Wang L (2012) Possible association of the western Tibetan Plateau snow cover with the decadal to interdecadal variations of northern China heatwave frequency. Clim Dyn 39:2393–2402. https://doi.org/10.1007/s00382-012-1439-4

Xie TJ, Li JP, Sun C, Ding RQ, Wang KC, Zhao CF, Feng J (2019) NAO implicated as a predictor of the surface air temperature multidecadal variability over East Asia. Clim Dyn 53:895–905. https://doi.org/10.1007/s00382-019-04624-4

Yeh SW, Lee EH, Min SK, Lee YH, Park IH, Hong JS (2021) Contrasting factors on the trends in hot days and warm nights over Northern Hemisphere land during summer. Weather Climate Extremes 34:100389. https://doi.org/10.1016/j.wace.2021.100389

You Q, Jiang Z, Kong L et al (2017) A comparison of heat wave climatologies and trends in China based on multiple definitions. Clim Dyn 48:3975–3989. https://doi.org/10.1007/s00382-016-3315-0

Zhao S, Li JP, Li Y (2015) Dynamics of an interhemispheric teleconnection across the critical latitude through a southerly duct during boreal winter. J Clim 28:7437–7456. https://doi.org/10.1175/JCLI-D-14-00425.1

Zhao S, Li JP, Li Y, Jin F-F, Zheng J (2019) Interhemispheric influence of Indo-Pacific convection oscillation on Southern Hemisphere rainfall through southward propagation of Rossby waves. Clim Dyn 52:3203–3221. https://doi.org/10.1007/s00382-018-4324-y

Zhou MZ, Wang HJ, Yang S, Fan K (2013) Influence of springtime North Atlantic oscillation on crops yields in Northeast China. Clim Dyn 41:3317–3324. https://doi.org/10.1007/s00382-012-1597-4

Zhu CW, Wang B, Qian WH, Zhang B (2012) Recent weakening of northern East Asian summer monsoon: a possible response to global warming. Geophys Res Lett 39:L09701. https://doi.org/10.1029/2012GL051155

Zuo J, Ren HL, Li W (2015) Contrasting impacts of the Arctic oscillation on surface air temperature anomalies in southern China between early and middle-to-late winter. J Clim 28:4015–4026. https://doi.org/10.1175/JCLI-D-14-00687.1